Calibration considerations for a reduced-timeline optimized approach for VNIR earth-orbiting satellites

Zachary Bergen, Joe Tansock
Space Dynamics Laboratory
1695 North Research Park Way, North Logan, UT 84341
Zachary.Bergen@sdl.usu.edu, Joe.Tansock@sdl.usu.edu

ABSTRACT

With the increasing number of commercial satellite constellations launching, the need for calibration remains as relevant as ever. Some of these instruments are built with COTS optical components and, given the number and need for timely calibration, a flexible, dynamic, and streamlined approach is necessary for reproducibility, regression testing, adaptability, and high-quality image data. We present a use case for a commercial VNIR payload and demonstrate techniques and a storyboard of our experience. We ran a calibration campaign on a 100" focal length telescope assembled in a payload of approximate 50kg containing a commercial Bayer pattern camera of medium resolution (6600x4400 pixels). We performed nonuniformity correction (NUC), focus estimation, camera parameter settings, off-axis scatter measurements, and an assessment of a charge-coupled device (CCD) smear. It is understood that there is a level of risk accepted in the commercial enterprise. In our case, the first two satellites out of a constellation of approximately100 satellites are intended for a proof-of-concept (POC) to facilitate a baseline of sensor performance and to provide a calibration template for the remaining satellites.

INTRODUCTION

The calibration of COTS components in a telescope requires a general approach that can be optimized quickly when areas of concern are found. The calibration steps must be agile in response to findings. It was decided to perform calibration testing with the sensor operated in a thermal vacuum chamber to enable performance testing at specific operating temperatures. Given the consideration of the warm up/cool down cycles necessary with thermal vacuum equipment, the approach must consider all of the dependencies and be able to switch measurement emphasis to make the best use of the timeline.

We chose specific steps based on schedule, priority, financial considerations, and equipment availability:

- Focus
- Focus Uncertainty
- Non-Uniformity Correction (NUC)
- Camera Parameter Settings
- Off-Axis Scatter Verification
- Assessment of CCD Smear

The Space Dynamics Laboratory (SDL) boasts a calibration facility that contains equipment for providing a full suite of calibration tests. The THOR vacuum chamber is large enough to contain a small satellite. The payload for this work weighs around 50 kg and fits easily inside the vacuum chamber. THOR enables us to synthesize the space environment to establish the behavior of the payload during the transition from Earth to orbit and a stable on-orbit environment.

Figure 1 shows the calibration engineers assembling the payload on its custom mount in the THOR chamber.

Figure 1: THOR configuration

The CCD sensor array produces a Bayer pattern of red, green, and blue (RGB) pixels. The Bayer pattern introduces additional considerations for calibration. Since the quantum efficiency of the three bands is different, we must take this into consideration for calculations/measurements such as white balance, focus extent, and power.

FOCUS

Method

The measurement configuration for focus consisted of a collimator mirror at infinity focus, a moveable pinhole aperture, and the telescope under test. The infinity focus of the collimator was quantified and verified using interferometry. In addition, the chamber window temperature gradient effects on the sensor focus were measured and accounted for in the sensor focus assessment.

The method to quantify the sensor's best (or infinity) focus was determined by quantifying an RGB NUC to normalize the RGB pixels and then following the steps shown below (normalize the RGB sensor response to the blackbody source used to back illuminate the pin hole located at the focus of the collimator). This enables subsequent pinhole response analyses.

1) For each pinhole image we:
    a. Performed dark correction
    b. Applied the RGB NUC
    c. Calculated an encircled energy figure of merit
    d. Stored the results
2) Performed focus analysis for payload best focus (i.e. infinity focus)
    a. Plotted encircled energy as a function of ground collimator focus setting
    b. Performed curve fit to determine the ground collimator focus that maximizes encircled energy
3) Related ground collimator focus to payload delta focus

The encircled energy figure of merit (EEFM) is defined as:

$$EncircledEnergy = \frac{\sum_{\sqrt{(i-i_c)^2+(j-j_c)^2} \le Rad} response_{i,j}}{\sum_{i,j} response_{i,j}} \quad (1)$$

where i and j are the indices over sub window and i_c and j_c are the intensity weighted centroid position. The EEFM quantifies the fraction of energy within a circle of pixels to the total energy of all pixels within the pinhole response window. For this analysis the radius is set to 4 pixels with a window size of 41x41 pixels which is made large enough to ensure the defocused pinhole response remains in the window. Based on measurement and optical modeling of a previous program (1), ensquared energy was an unbiased estimator of best focus compared to full width half maximum (FWHM).

For the focus analyses, the focus evaluation was performed at the center of the FOV and repeated at the corners of the focal plane array (FPA). This was done to quantify tip or tilt of the FPA. To compute the RGB NUC, each pixel is averaged for 10 illuminated images and averaged for 10 dark images. The RGB NUC correction disk response is calculated as the difference between the averaged illuminated image and average dark image are normalized. We produced the RGB NUC corrected image by dividing the dark offset corrected pin hole response by the RGB NUC. Figure 2 shows this sequence for correcting an image for focus assessment.

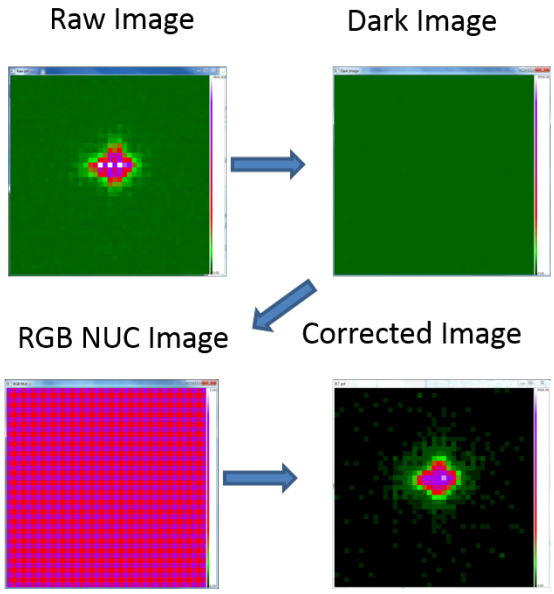

Figure 2: Sequence for focus image correction

The equipment setup for focus measurement is shown in Figure 3. An off-axis parabolic collimator mirror was placed at/near the focal point aligned with the boresight of the payload telescope. A moveable pinhole was placed in the optical path and measurements of EEFM are taken as the pinhole was moved. The relationship between the focus difference of the collimator mirror and the payload focus was established. We calculate the major sources of measurement error and propagate these errors to constrain the accuracy of the focus measurement.

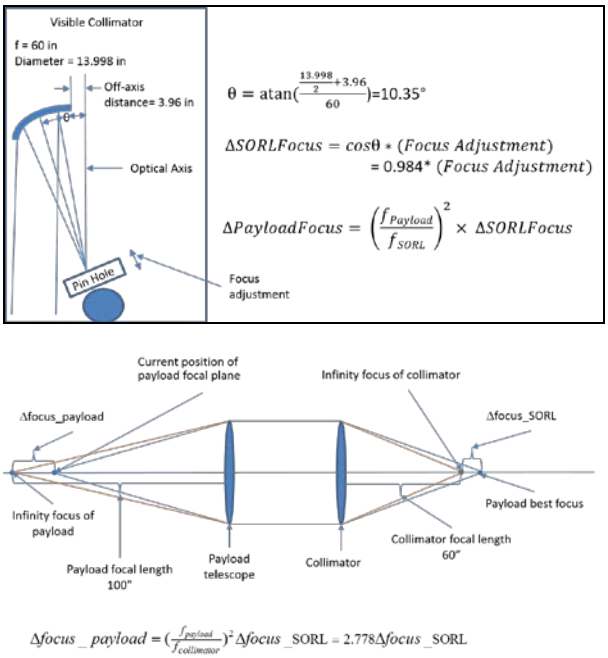

Figure 3: Focus measurement

After recording several images and correcting them, we are able to calculate the EEFM and plot vs the visible collimator focus. An example graph of measurements is shown in Figure 4.

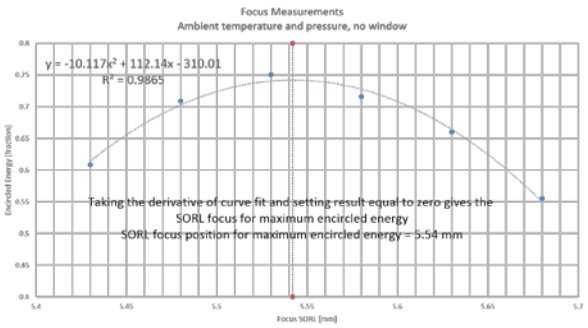

Figure 4: Sequence for focus image correction

Results

Referring to Figure 4, we are able to solve for the SORL focus position at the maximum EERM (5.54 mm). Given the relationship between SORL focus and payload focus the payload focus error is multiplied by 2.778 (15.39 mm). This particular result is not as important as the process of determining focus. It is customary to characterize system specifications that are assumed to need adjustment as the other aspects of the calibration are recorded. In this instance, the focus analysis results in the need to investigate experimental sources of error. Our particular result points to either a payload re-design for the space environment or changes in the telescope to further reduce sensitivity to temperature and pressure.

Figure 5 shows a couple of exposures at two different focus settings. The energy distribution moves from a ring pattern to a more focused energy distribution yet does not ever reach a small spot size.

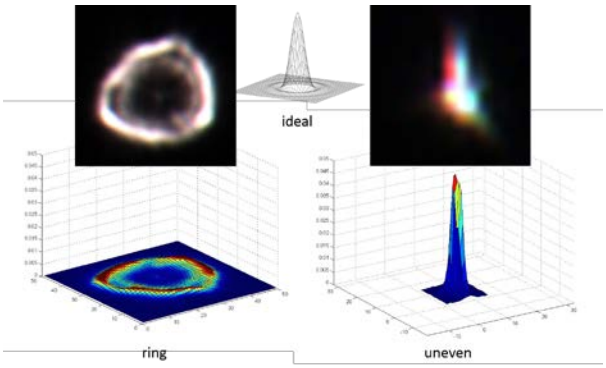

Figure 5: Images for two different focus settings

FOCUS UNCERNTAINTY

Method

To understand the uncertainty of focus measurements, we investigated sources of focus uncertainty due to the experimental setup. Table 1 lists the areas we investigated for contribution to focus error.

Table 1: Sources of focus uncertainty

Source	Description	Uncertainty (mm)
SORL infinity focus	Accuracy of infinity focus of SORL mirror	0.05
THOR visible window[1]	THOR window mount	0.30
Quick look and detailed delta	Potential improvement of focus estimate using quick look vs. data analysis	0.167
Off-axis SORL mirror	Effect of off-axis geometry or SORL mirror	0.083
SORL to payload delta focus	Ratio of focal length squared for SORL to payload delta focus	0.06
Depth of payload focus	Theoretical depth of field	0.103
RSS total	Combination of all error sources	0.38

Methods have been employed to reduce window temperature gradients but a conservative estimate of uncertainty is used for this uncertainty analysis

Results

Table 1 shows the results of the focus uncertainty. The root squared sum (RSS) result is 0.38 mm and quantifies the limit on our focus measurement accuracy. It should be noted the dominating focus uncertainty contribution is due to temperature gradients on the vacuum chamber window. For subsequent testing, this uncertainty was further reduced by measuring and minimizing window temperature gradients during test. This type of uncertainty evaluation is necessary to verify focus results.

NUC (MEASUREMENT, VALUE, AND CAMERA TEMP EVALUATION)

Method

We used an integrating sphere set to provide a uniform source at the aperture of the telescope. To evaluate changes in NUC as a function of camera temperature, we chose three different settings for evaluating the NUC.

Results

Table 2 shows the results for the dependency on the mean pixel value on camera temperature. These results show that the NUC established using integrating sphere exposure data for expected operating temperatures will work for the entire range of anticipated on-orbit operational temperatures.

Table 2: NUC temperature sensitivity analysis

Temperature ©	Mean (counts)	Std Dev (counts)
17.3	6.02	0.08
21.8	6.00	0.09
34.8	6.01	0.12

In addition to the temperature dependencies, we are able to streamline subsequent tests on the payload and other satellites anticipated in the constellation. This is because we find ranges of illumination matched to response levels and can reduce the number of exposures necessary to characterize the payload.

Since the NUC characterizes the telescope illumination along with the CCD response (i.e. the "fingerprint" of the sensor) it is unique to each satellite. Our focus was to investigate the efficacy of using a single NUC for every image. Since the temperature sensitivity was small it is possible, with this payload, to use a single NUC file. The absolute worst-case scenario revealed a 2 count variation on an 8-bit camera CCD pixel output setting. The nominal result on-orbit is expected to be a fraction of a single count.

CAMERA PARAMETER SETTINGS FOR ON-ORBIT OPERATIONS

Method

The commercial camera used in the payload has settings such as gain, offset, exposure, and white balance. Some of these can be programmed into non-volatile memory. We investigated the camera response given expected TOA radiance values to find reasonable on-orbit settings and verify the proper working order of the camera in the telescope configuration. While the number of settings is too large to report here, we selected a few settings of interest. Most of the experiments revealed congruence with the reported factory results.

To simulate on-orbit operation we installed a heater on the camera to control the camera temperature while in the vacuum test chamber. Like most commercial cameras, we were able to change the settings with the provided software and interface cable to the camera port. Figure 6 shows the camera with temperature sensors attached (top) and the control cable attached to the laptop computer running the provided camera control software (bottom).

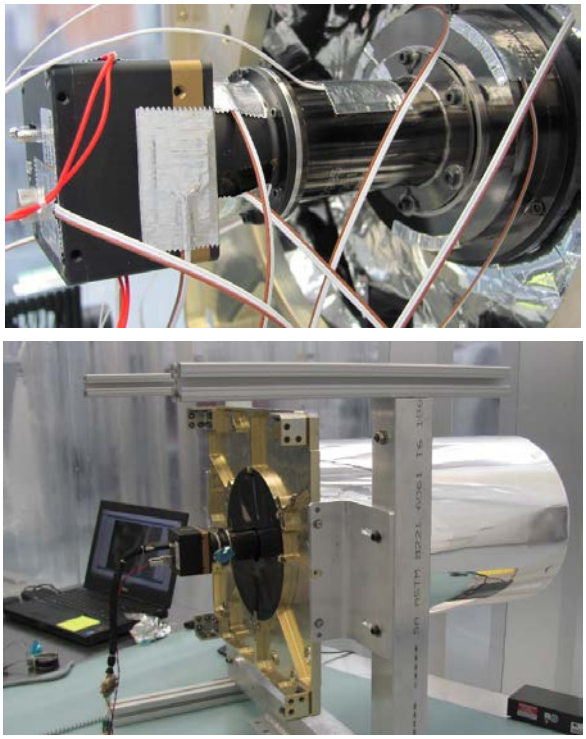

Figure 6: Camera with sensors

The procedure for testing the camera settings is to simply record images for a range of settings from the following capabilities (Table 3) and process the resulting imagery for performance in terms of signal to noise (SNR) fluctuations. The goal is to find an acceptable frame capture rate that gives the highest SNR.

Table 3: Camera settings

Setting	Range
Temperature	Variable Continuous
AGC	ON/OFF
AEC	ON/OFF
Luminance Level Threshold	Counts
Analog Gain	Variable
Exposure Time	Variable
Pre-Amp Gain	-3/0/+3 dB
Bit Depth	8/12
Framelink Option	Mono or Bayer
White Balance	ON/OFF
Black Compensation	ON/OFF
Tap Balance	ON/AUTO
DPC	Off/Static/Dynamic/Combined
HPC	Off/Static/Dynamic/Combined

Results

The camera parameter setting imagery collects reveal multidimensional data surfaces that contain areas for optimizing SNR, exposure, and gain settings among others. For the purposes of this discussion, we concentrate on the exposure and SNR.

Figure 7 shows the dependency of the SNR on various gain and exposure settings. While the response (dashed red line) is relatively constant, the SNR varies and displays a peak which is useful for combining with anticipated exposure times on orbit given the relative velocity of the spacecraft. Since Figure 7 is not complete enough to see the dependencies of uncouples gain/exposure settings, Figure 8 is a result of creating an SNR surface with gain and exposure as independent variables.

Figures 7 and 8 provide a compendium of multivariate test outputs and enable us to isolate operating regions for the telescope given system constraints such as maximum exposure time. For example, Figure 7 shows that we can maintain a high SNR with gains below 7 and exposure times above 1288 μs. If the exposure time is not within specifications, we can see that we would have to sacrifice SNR in favor of a shorter exposure time. If the SNR is still within specification, then the data reveals how the SNR behaves in the tradeoff. Figure 8 separates the horizontal axis in Figure 7 so that we can include more combinations of collects gain and exposure times vs SNR. We could put a threshold on SNR and easily see the allowable operating region for exposure and gain.

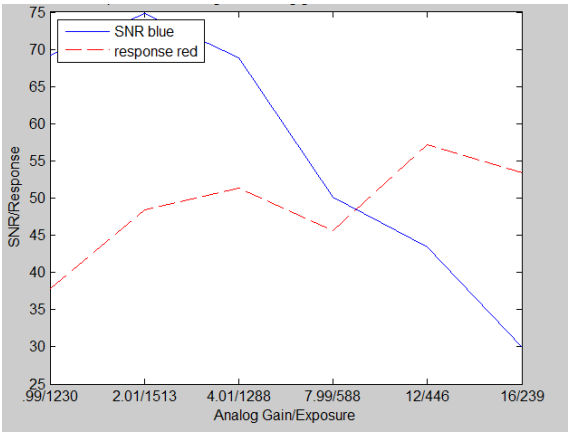

Figure 7: SNR/response vs analog gain/exposure

Figure 8 reveals a fairly planar surface with expected results where the SNR increases with exposure time and decreases with gain. The figure is useful to show the trend, and settings for on-orbit operation of the payload may be set with a threshold on required SNR and exposure time limits.

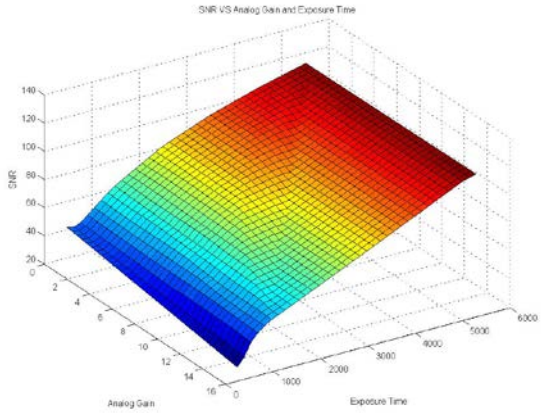

Figure 8: SNR surface vs analog gain and exposure

OFF AXIS SCATTER VERIFICATION

Method

This test is considered a verification because the data may be used to identify unexpected and undesirable off-axis scatter response rather than provide a detailed assessment.

Given the focus measurement results, we decided to direct our efforts to other aspects of payload characterization that are not as sensitive to focus, such as the off-axis scatter and focal plane response effects, including smear.

For this test, the payload off-axis scatter response is checked by varying the distance between the integrating sphere and payload for a constant integrating sphere setting. For all separation distances, the field of view (FOV) is completely overfilled by the integrating sphere. Because of the geometry shown in Figure 9 when the payload is close to the integrating sphere, the telescope is illuminated with light at angles larger than the FOV. When the separation distance is large, the light with angles larger than the FOV are at a minimum.

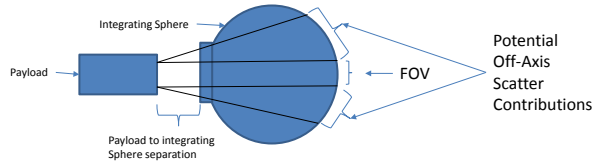

Figure 9: Off-axis scatter configuration

To create a useful range of off-axis angles, we look at the extremes for stray light given a nadir viewing geometry. Figure 10 shows the calculation for a satellite at 450 km orbit.

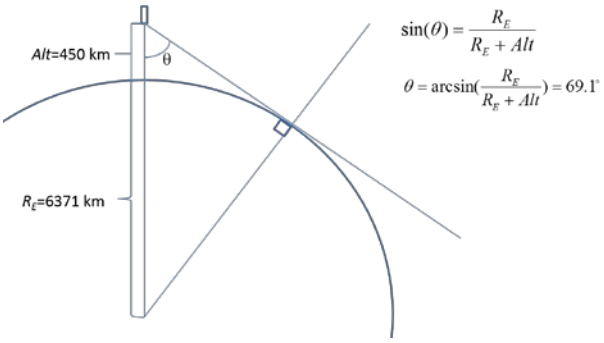

Figure 10: Off-axis viewing geometry

Results

The off-axis scatter verification results are shown in Table 4.

Table 4: Off-axis scatter results

Off axis angle [deg]	Off axis angle uncertainty [deg]	Mean Response [counts]	Mean Pdif [%]	Stddev [%]
Region	Full array			
1.1	2.4E-03	1149.5	0.0	0.0
5.2	3.3E-02	1210.1	5.3	1.1
9.7	1.1E-01	1239.4	7.8	1.2
20.1	4.0E-01	1286.6	11.4	1.4
33.2	1.1E+00	1313.8	13.5	1.5
53.8	2.3E+00	1328.7	14.5	1.5
69.8	3.1E+00	1335.7	15.0	1.5

There is an increase in array mean response from 0 to about 15% as a function of off-axis angle. This does not show the structure of the response. Figure 11 is an image of the structure of the off-axis scatter. Such structure information can be useful in designing baffles or other aspects of the telescope design to minimize the scatter if it is significant enough to affect image quality.

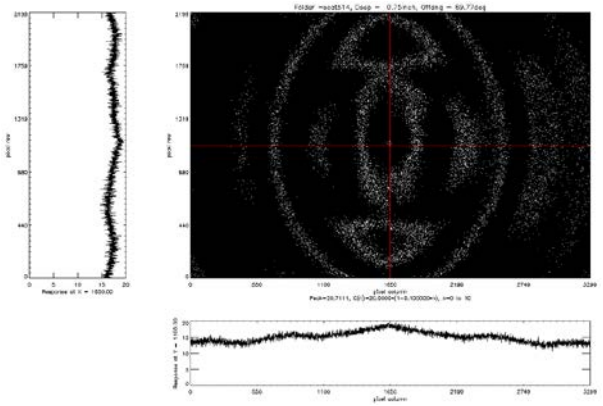

Figure 11: Off-axis scatter structure

ASSESSMENT OF CCD SMEAR

The CCD in the camera has a saturation feature to prevent blooming where any excess charge above the well potential is bled into the substrate. There is a limit on the smear with a factory measurement of -100 dB. During out test, we discovered a vertical smear due to a relatively bright illumination in the center of the image. Figure 12 illustrates smear for a bright center disk illumination. The lighter vertical bar in Figure 12 is the smear and not a result of direct illumination.

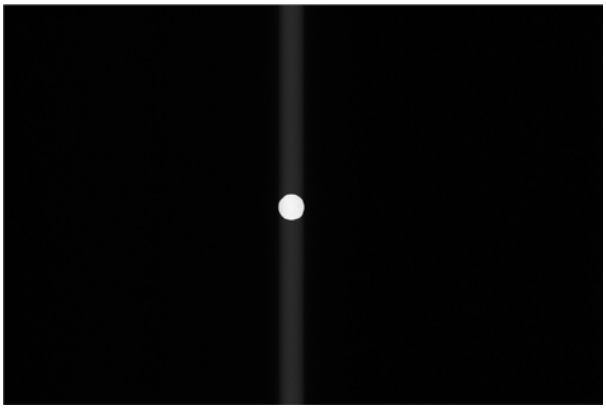

Figure 12: Smear

Method

The method of smear assessment involves bright illumination with a resolved response (not pinhole) of adequate illumination to create the effect.

Results

Smear is a constant value in the vertical direction. Assuming that the smear is independent of the source position on the focal plane, then the NUC should not be affected. The characteristic of the CCD smear is that it is located in the vertical directions (above and below) pixels that are directly illuminated by the source. The smear amplitude appears to be dependent on the source level rather than pixel RGB response.

The smear is a known aspect of most CCD sensors and the recommendation is to evaluate source brightness and exposure times to limit the effect. It is reasonable to expect that some Earth view images will contain CCD smear.

Conclusion

The essential element of agile calibration involves a tight loop between experiment, theory, and timely data processing. We presented a compressed 10-day calibration campaign with concomitant data processing guiding the subsequent steps.

We ran a calibration campaign on a visible and VNIR imaging commercial payload. We characterized nonuniformity correction (NUC), performed focus estimation, exercised camera parameter settings, characterized off-axis scatter measurements, and performed an assessment of CCD smear. It is understood that there is a level of risk that is acceptable in many commercial enterprises. For this program, calibration parameters were chosen with considerations of schedule, priority, financial, and equipment availability. This enabled establishing an acceptable calibration and test campaign given the constraints of the project and reducing risk of discovering a technical issue before incurring launch and/or deployment expenses.

References

1. Focus Optimization of the SPIRIT III Radiometer, *Opt. Eng*. 36(11), 2936-2942 (Nov 01, 1997). doi:10.1117/1.601533.
2. Wyatt, C.L., Radiometric Calibration: Theory and Methods, Academic Press, New York, 1978.